

1 **Nonlinear vibration analysis of a rotor system with parallel and angular** 2 **misalignments under uncertainty via a Legendre collocation approach**

3 **Chao Fu^{1,2†}, Yongfeng Yang¹, Kuan Lu¹, Fengshou Gu²**

4 ¹Institute of Vibration Engineering, Northwestern Polytechnical University, Xi'an 710072, China

5 ²Centre for Efficiency and Performance Engineering, University of Huddersfield,
6 Queensgate, Huddersfield, HD1 3DH, United Kingdom

7 [†]Corresponding author: fuchao0606@mail.nwpu.edu.cn; fuchaouk@gmail.com

8 **Abstract**

9 In this paper, the propagation of bounded uncertainties in the dynamic response of a misaligned rotor is
10 investigated using a Legendre collocation based non-intrusive analysis method. A finite element rotor
11 model is used and the parallel and angular misalignments are modelled by additions of stiffness and
12 force terms to the system. A simplex meta-model for the harmonic solutions of the vibration problem is
13 constructed to take into account the uncertainties. The influences of uncertainties in the fault parameters
14 are analysed and the calculation performance of the interval method is validated. Different propagation
15 mechanisms of the uncertainties are observed in the interval responses and discussed in case studies.
16 The results of this study will promote the understandings of the nonlinear vibrations in misaligned rotor
17 systems with interval variables.

18 **Keywords:** rotor; misalignment; bounded uncertainty; harmonic response; Legendre collocation

19 **1. Introduction**

20 Rotating machineries have wide applications in industrial fields and play an important role in both the
21 civil economics and military services (Roy and Meguid 2018; Biswas and Ray 2013; Lu et al. 2018).
22 Typical faults such as a crack may occur during operation, which will cause harmful vibrations (Ma et
23 al. 2015a). The stability of rotor systems mounted on journal bearings with multi slip zones was studied
24 by Bhattacharya et al. (2017). Li et al. (2019) investigated the nonlinear dynamics of a rotor supported
25 by nonlinear supports at both ends and the effect of rubbing was analysed. Residual bow was found to
26 have a significant effect on the first order critical speed of the geared system with stiff viscoelastic
27 supports (Kang et al. 2011). Misalignment is deemed to be the second most common fault after out of
28 balance and they often exist simultaneously (Patel and Darpe 2009; Wang and Jiang 2018; Srinivas et
29 al. 2019). Assembling error, long time operation and thermal effects are contributory to these faults.
30 Extra reacting forces and moments will be generated and the dynamics including stability of the rotor
31 system can be significantly influenced (Ma et al. 2015b; Tuckmantel and Cavalca 2019; Al-Hussain
32 2003). In rotor systems, there are generally two types of misalignment, i.e. the parallel misalignment
33 and the angular misalignment. The modelling methods and various dynamic behaviors in misaligned
34 rotors have been investigated by many researchers worldwide. Li et al. (2012) established the

35 mathematical model of a rotor system in aero-engine subject to misalignment and unbalance coupling
36 faults. Wang et al. (2015) used an additional stiffness term to simulate the effect of angular misalignment
37 and derived the motion equations of a four-degrees-of-freedom rotor system. Li et al. (2016; 2017)
38 modelled angular misalignment based on the geometric constraints between the adjacent coordinates.
39 Lees (2007) proposed the modelling method for parallel misalignment using the Lagrange's formulation
40 where shafts are connected by a number of bolts. The technique was further used to analyse angular
41 misalignment (Didier et al. 2012a). Sinha et al. (2004) proposed an estimation method for the
42 misalignment and unbalance faults based on only one run-down process. Its robustness was verified via
43 sensitivity analysis on rotor bearing models. Xu and Marangoni (1994) carried out the experimental
44 validation for dynamic characteristics of an unbalanced rotor system with misalignment and revealed
45 some in-depth vibration behaviours at the $2 \times$ rotating speed of the system.

46 In the design stage, it is very hard to accurately simulate the actual operational conditions and physical
47 parameters will have critical impacts on the vibration characteristics of rotor systems. Errors and extra
48 variations may be introduced in manufacturing, service and maintenance periods (Liu et al. 2016; Jiang
49 et al. 2012). In other words, there are ubiquitous uncertainties in the physical models, excitations and
50 classic faults. The corresponding dynamic behaviours can deviate from the design values and further
51 cause instabilities or severe failures (Fu et al. 2017). This is especially true for misaligned rotors, which
52 may be affected by manual assemble errors or small defects in couplings. In engineering, it often
53 happens that the vibration will deteriorate when a well-balanced rotor is reassembled. The uncertainty
54 analysis for rotordynamics has attracted attention in recent years. Some studies have been reported in
55 the literature (Yang et al. 2019; Lu et al. 2019; Sinou et al. 2018; Fu et al. 2018a, 2018b; Didier et al
56 2012b; Koroishi et al. 2012; Ritto et al. 2011; Sinou and Faverjon 2012), which were devoted to
57 investigating the linear and nonlinear dynamics of rotor systems under various uncertain conditions
58 based on both the stochastic and non-probabilistic approaches. More specifically, Li et al. (2016; 2017)
59 studied the random nonlinear vibration characteristics of a rotor system with angular misalignment and
60 nonlinear bearings using the Polynomial Chaos Expansion (PCE). Multiple typical faults in a rotor
61 system, including the parallel and angular misalignments, were considered by Didier et al. (2012a) and
62 the influences of the stochastic fault parameters were investigated using the PCE. Li et al. (2012) and
63 Wang et al. (2015) employed the Taylor interval method to reveal the uncertain dynamics of misaligned
64 dual rotors simplified from the aero-engine. Some important factors should be considered in the
65 uncertainty propagation analysis of misaligned rotor systems, i.e. the application prerequisites and
66 implementation convenience of the propagation methods, the accuracy of the physical model and the
67 underlying computational efficiency. The distribution model of uncertainty should be established in the
68 probability-based methods or hypothesis should be made, which could be subjective. The Taylor
69 interval analysis method is derivative-based and intrusive, which is only suitable for small range

70 uncertainty and is difficult to adapt to large-scale models or high-order problems. Therefore, they can
71 only be used in systems with a few degrees of freedom. This paper will focus on the uncertainty
72 propagation analysis of a finite element rotor model with both the parallel and angular misalignments.
73 A Legendre collocation based non-intrusive interval surrogate is proposed for this purpose, which
74 avoids complicated approximation theory and derivation operations in the previous methods. Large
75 variations in the uncertainties can be applied. Efforts aimed at reducing the computation burden are
76 incorporated to deal with multi-dimensional uncertainties. The high efficiency and accuracy, as well as
77 the uncomplicated implementation of the method will be demonstrated via case studies. The variability
78 patterns of the responses due to the uncertainties in the two types of misalignment will be revealed.
79 The remainder of the content is as follows. The modelling process of the parallel and angular
80 misalignments will be briefly explained in Section 2. Section 3 presents the steps and principles of the
81 uncertainty propagation method. Numerical simulation with uncertainties in the fault parameters will
82 be given in Section 4. Some conclusions are summarised in the last section.

83 **2. Misalignment modelling and the deterministic motion equation**

84 The finite element method (FEM) has been widely used to model the rotating systems and establish the
85 governing equations of motion in relation to the lateral vibration (Friswell et al. 2010). For a general
86 rotor-disk-bearing system, the modelling of the Euler beam elements, mass disks and linear isotropic
87 bearing elements is standard. The matrices for different typical elements and the assemblage technique
88 will not be described in the current study and the readers are referred to Friswell et al. (2010) for further
89 instructions. Generally, the governing motion equation of a rotor-disk-bearing system can be
90 represented as

$$91 \quad \mathbf{M}\ddot{\mathbf{q}}(t) + (\mathbf{C} + \omega\mathbf{G})\dot{\mathbf{q}}(t) + \mathbf{K}\mathbf{q}(t) = \mathbf{F}(t) \quad (1)$$

92 where \mathbf{M} , \mathbf{C} , \mathbf{K} and \mathbf{G} are, respectively, the global mass, damping, stiffness and gyroscopic
93 matrices of the system. The acceleration, velocity and displacement vectors are denoted by $\ddot{\mathbf{q}}(t)$, $\dot{\mathbf{q}}(t)$
94 and $\mathbf{q}(t)$, respectively. $\mathbf{F}(t)$ is the unbalance and gravitational forces. ω represents the angular
95 speed of the shaft. All quantities given in Eq. (1) are formulated in the fixed coordinate system.

96 *2.1. Parallel misalignment*

97 In this subsection, the effects of the parallel misalignment on the system will be modelled. The two
98 rotors connected by coupling with N bolted joints are assumed to be operating at a synchronized rotating
99 speed. The bolts are distributed on a circle at a radius r_p from the shaft centerline and they have a
100 transverse stiffness k_t . Suppose the centerlines of the two shafts have a relative vertical displacement
101 δ_p , the schematic configuration of the fault is illustrated in Fig. 1. Obviously, the effects are
102 exaggerated here to show the relationship although the displacement is generally small in reality.

103 As the bolts are evenly distributed in a circumference, their angles can be defined as

$$\alpha_i = \frac{i-1}{N} \pi, \quad i=1, 2, \dots, N \quad (2)$$

According to the geometrical relationship, the position of the i th bolt on the two rotors in fixed coordinate frame can be given as (Lees 2007; Didier et al. 2012a)

$$\mathbf{OM}_1^i = \begin{bmatrix} v \\ w \\ 0 \end{bmatrix} + \begin{bmatrix} -r \sin(\omega t + \alpha_i) \\ r \cos(\omega t + \alpha_i) \\ r\varphi \cos(\omega t + \alpha_i) + r\beta \sin(\omega t + \alpha_i) \end{bmatrix} \quad (3)$$

$$\mathbf{OM}_2^i = \begin{bmatrix} -r \sin(\omega t + \alpha_i) - \delta_p \sin(\omega t) \\ r \sin(\omega t + \alpha_i) - \delta_p (1 - \cos(\omega t)) \\ 0 \end{bmatrix} \quad (4)$$

where $[v \ w \ \varphi \ \beta]^T$ denotes the nodal lateral displacement vector of the coupling and t is time. Then the sum of strain energy of bolts can be given as

$$E_{pm} = \frac{1}{2} N k_t [(v + \delta_p \sin(\omega t))^2 + (w + \delta_p (1 - \cos(\omega t)))^2] \quad (5)$$

After the Lagrange's operation, the effects of parallel misalignment will be represented by an additional stiffness term and a force term on the coupling node (Didier et al. 2012a; El-Mongy and Younes 2018)

$$\mathbf{K}_{pm} = N k_t \text{diag}(1, 1, 0, 0) \quad (6)$$

$$\mathbf{F}_{pm} = N k_t \delta_p [\sin(\omega t), 1 - \cos(\omega t), 0, 0]^T \quad (7)$$

2.2. Angular misalignment

The angular misalignment can be modelled similarly to the previous method. The bolts will have an axial stiffness k_a and the first one will have the stiffness $k_a + k'$ in z direction (Didier et al. 2012a). Suppose the magnitude of angular misalignment is δ_a , a schematic diagram showing the configuration of the fault is presented in Fig. 2. Similarly, the magnitude of the angular misalignment is small and it is intentionally magnified.

The positions of bolts are calculated in the fixed frame as

$$\mathbf{O}_2 \mathbf{M}_2^i = \begin{bmatrix} -r \sin(\omega t + \alpha_i) \\ r \cos(\omega t + \alpha_i) \\ r \delta_a \cos(\omega t + \alpha_i) \end{bmatrix} \quad (8)$$

Then the strain energy of bolts can be given as

$$E_{am} = \sum_i^N \frac{1}{2} r^2 k_i [(\varphi - \delta_a) \cos(\omega t + \alpha_i) + (\beta \cos(\omega t + \alpha_i))]^2 \quad (9)$$

By Lagrange's calculation, one can describe the effects of angular misalignment using a time-variant stiffness term and a two-order harmonic force term (Didier et al. 2012a)

$$\mathbf{K}_{am} = \frac{1}{2}(3k_a + k')r^2 \begin{bmatrix} 0 & & & \\ & 0 & & \\ & & 1 & \\ & & & 1 \end{bmatrix} + \frac{1}{2}k'r^2 \begin{bmatrix} 0 & & & \\ & 0 & & \\ & & \cos(2\omega t) & \sin(2\omega t) \\ & & \sin(2\omega t) & -\cos(2\omega t) \end{bmatrix} \quad (10)$$

$$\mathbf{F}_{pm} = -\frac{1}{2}r^2\delta_p[0, 0, 3k_a + k'(1 + \cos(2\omega t)), k'\sin(2\omega t)]^T \quad (11)$$

128
129
130 Considering the effects of the parallel and angular misalignments on the rotor, the motion equations of
131 the misaligned system can be written as

$$\mathbf{M}\ddot{\mathbf{q}} + (\mathbf{C} + \omega\mathbf{G})\dot{\mathbf{q}} + (\mathbf{K}_0 + \mathbf{K}_c \cos(2\omega t) + \mathbf{K}_s \sin(2\omega t))\mathbf{q} = \mathbf{F}_0 + \mathbf{F}_{c1} \cos(\omega t) + \mathbf{F}_{s1} \sin(\omega t) + \mathbf{F}_{c2} \cos(2\omega t) + \mathbf{F}_{s2} \sin(2\omega t) \quad (12)$$

133 where \mathbf{K}_0 is a constant stiffness matrix, including \mathbf{K} in Eq. (1), the stiffness in Eq. (6) and the
134 constant part in Eq. (10). \mathbf{K}_c and \mathbf{K}_s are the stiffness matrices of the second order harmonics. \mathbf{F}_0
135 is the constant part of the forces on the system. \mathbf{F}_{c1} and \mathbf{F}_{s1} are the force amplitudes of the first order
136 harmonics whilst \mathbf{F}_{c2} and \mathbf{F}_{s2} are those of the second order harmonics.

137 Given the form of Eq. (12), the harmonic balance method (HBM) (Nayfeh and Mook 2008), a fast
138 method for steady-state solutions, can be conveniently employed to solve the dynamic response of the
139 system. The forces on the system shown in the right hand side of Eq. (12) are already in harmonic form.
140 The displacement vector can then be expressed in finite Fourier expansion

$$\mathbf{q}(t) = \mathbf{A}_0 + \sum_{k=1}^n (\mathbf{A}_k \cos(k\omega t) + \mathbf{B}_k \sin(k\omega t)) \quad (13)$$

142 where n is the truncation order. Order 4 will be adequate for the present study according to previous
143 nonlinear analyses of faulty rotor systems (Sinou and Faverjon 2012; Tai et al. 2015; Yang et al. 2019).
144 Then magnitude of the j -th order harmonic component of the dynamic response can be calculated as

$$\sqrt{\mathbf{A}_k^2 + \mathbf{B}_k^2}, k = 0, 1, \dots, n \quad (14)$$

146 Submit Eq. (13) into Eq. (12) and balance the coefficients of the same order harmonic terms, it will
147 generate a set of linear equations

$$\mathbf{H}\mathbf{X} = \mathbf{\Gamma} \quad (15)$$

149 where

$$\mathbf{X} = [\mathbf{A}_0, \mathbf{A}_1, \mathbf{B}_1, \dots, \mathbf{A}_n, \mathbf{B}_n]^T \quad (16)$$

$$\mathbf{\Gamma} = [\mathbf{F}_0, \mathbf{F}_{c1}, \mathbf{F}_{s1}, \mathbf{F}_{c2}, \mathbf{F}_{s2}, \mathbf{0}, \dots, \mathbf{0}]^T \quad (17)$$

153

$$\mathbf{H} = \begin{bmatrix}
\mathbf{K}_0 & \mathbf{0} & \mathbf{0} & 0.5\mathbf{K}_1 & 0.5\mathbf{K}_2 & \mathbf{0} & \mathbf{0} & \mathbf{0} & \mathbf{0} & \dots & \mathbf{0} & \mathbf{0} \\
\mathbf{0} & \Lambda^{(1)} + 0.5\mathbf{K}_1 & \tilde{\Lambda}^{(1)} + 0.5\mathbf{K}_2 & \mathbf{0} & \mathbf{0} & 0.5\mathbf{K}_1 & 0.5\mathbf{K}_2 & \mathbf{0} & \mathbf{0} & \dots & \mathbf{0} & \mathbf{0} \\
\mathbf{0} & -\tilde{\Lambda}^{(1)} + 0.5\mathbf{K}_2 & \Lambda^{(1)} - 0.5\mathbf{K}_1 & \mathbf{0} & \mathbf{0} & -0.5\mathbf{K}_2 & 0.5\mathbf{K}_1 & \mathbf{0} & \mathbf{0} & \dots & \mathbf{0} & \mathbf{0} \\
2\mathbf{K}_1 & \mathbf{0} & \mathbf{0} & \Lambda^{(2)} & \tilde{\Lambda}^{(2)} & \mathbf{0} & \mathbf{0} & 0.5\mathbf{K}_1 & 0.5\mathbf{K}_2 & \ddots & \mathbf{0} & \mathbf{0} \\
2\mathbf{K}_2 & \mathbf{0} & \mathbf{0} & -\tilde{\Lambda}^{(2)} & \Lambda^{(2)} & \mathbf{0} & \mathbf{0} & -0.5\mathbf{K}_2 & 0.5\mathbf{K}_1 & \ddots & \vdots & \vdots \\
\mathbf{0} & 0.5\mathbf{K}_1 & 0.5\mathbf{K}_2 & \mathbf{0} & \mathbf{0} & \Lambda^{(3)} & \tilde{\Lambda}^{(3)} & \mathbf{0} & \mathbf{0} & \ddots & \mathbf{0} & \mathbf{0} \\
\mathbf{0} & -0.5\mathbf{K}_2 & 0.5\mathbf{K}_1 & \mathbf{0} & \mathbf{0} & -\tilde{\Lambda}^{(3)} & \Lambda^{(3)} & \mathbf{0} & \mathbf{0} & \ddots & 0.5\mathbf{K}_1 & 0.5\mathbf{K}_2 \\
\mathbf{0} & \mathbf{0} & \mathbf{0} & 0.5\mathbf{K}_1 & 0.5\mathbf{K}_2 & \mathbf{0} & \mathbf{0} & \Lambda^{(4)} & \tilde{\Lambda}^{(4)} & \ddots & -0.5\mathbf{K}_2 & 0.5\mathbf{K}_1 \\
\mathbf{0} & \mathbf{0} & \mathbf{0} & -0.5\mathbf{K}_2 & 0.5\mathbf{K}_1 & \mathbf{0} & \mathbf{0} & -\tilde{\Lambda}^{(4)} & \Lambda^{(4)} & \ddots & \mathbf{0} & \mathbf{0} \\
\vdots & \vdots & \vdots & \ddots & \ddots & \ddots & \ddots & \ddots & \ddots & \ddots & \mathbf{0} & \mathbf{0} \\
\mathbf{0} & \mathbf{0} & \mathbf{0} & \mathbf{0} & \dots & \mathbf{0} & 0.5\mathbf{K}_1 & 0.5\mathbf{K}_2 & \mathbf{0} & \mathbf{0} & \Lambda^{(n)} & -\tilde{\Lambda}^{(n)} \\
\mathbf{0} & \mathbf{0} & \mathbf{0} & \mathbf{0} & \dots & \mathbf{0} & -0.5\mathbf{K}_2 & 0.5\mathbf{K}_1 & \mathbf{0} & \mathbf{0} & -\tilde{\Lambda}^{(n)} & \Lambda^{(n)}
\end{bmatrix} \quad (18)$$

156 where $\Lambda^{(s)} = \mathbf{K}_0 - (s\omega)^2 \mathbf{M}$ and $\tilde{\Lambda}^{(s)} = s\omega(\mathbf{C} + \omega\mathbf{G})$, $s=1, 2, \dots, n$. Then the unknown Fourier
157 coefficients, i.e. the steady-state dynamic responses, can be solved by Eq. (15).

158 3. Legendre collocation approach for uncertainty quantification

159 In the above modelling, uncertainties in the fault parameters are not included. This section will establish
160 the propagation model of bounded uncertainties in the harmonic responses. As discussed previously,
161 the non-intrusive and non-probabilistic uncertainty propagation procedures will prevail in complicated
162 engineering systems with little prior statistic information. Some interval analysis methods and surrogate
163 modelling techniques (Qiu and Wang 2003; Wu et al. 2013, 2016; Elishakoff and Sarlin 2016; Soize
164 2001; Qi and Qiu 2012) have been proposed for dynamic analysis of the uncertain truss structures and
165 multibody systems. Here, a Legendre collocation scheme is proposed to establish a simple meta-model
166 for the uncertain harmonic solutions. Firstly, the uncertain-but-bounded magnitude of the parallel
167 misalignment is expressed in interval form

$$168 \quad \delta_p^I = [\delta_p^c - \alpha_1 \delta_p^c, \delta_p^c + \alpha_1 \delta_p^c] \quad (19)$$

169 where superscripts I and c denote the interval quantity and its nominal value. α_1 is the uncertainty
170 range indicator for the parallel misalignment. Similarly, the uncertain magnitude of the angular
171 misalignment can also be written as

$$172 \quad \delta_a^I = [\delta_a^c - \alpha_2 \delta_a^c, \delta_a^c + \alpha_2 \delta_a^c] \quad (20)$$

173 where α_2 is its uncertainty indicator. More indicators will be generated if other physical parameters
174 are to be considered uncertain and a standard uncertain variable vector $\boldsymbol{\alpha} = \{\alpha_1, \alpha_2, \alpha_3, \dots\}$ can be
175 defined, which represents all the indicators. In the presence of interval parameters, the response output
176 of the rotor will also be uncertain. The harmonic solutions in Eq. (15) can be expressed as

$$177 \quad \begin{cases} \mathbf{A}_i^I = [\underline{\mathbf{A}}_i, \overline{\mathbf{A}}_i], i=0, 1, \dots, n \\ \mathbf{B}_j^I = [\underline{\mathbf{B}}_j, \overline{\mathbf{B}}_j], j=1, 2, \dots, n \end{cases} \quad (21)$$

178 where an underscore represents the lower bound (LB) and an overbar denotes the upper bound (UB).
179 Solving the uncertain dynamic problem is equivalent to determining the bounds of the interval harmonic
180 solutions expressed in Eq. (21). The meta-modelling technique can be used for this purpose. In the

181 following, the interval modelling method for any harmonic solutions of interest will be explained. It
 182 could be either the Fourier coefficient of a single component or all of them in a row. Naturally, the
 183 uncertain solution will be a function of the vector $\boldsymbol{\alpha}$, which can be denoted as $f(\boldsymbol{\alpha})$.

184 To establish the surrogate function, the basics of the Legendre orthogonal series should be described.
 185 The recursive relationships of Legendre polynomials are as follows

$$186 \quad \begin{cases} L_0(x) = 1, & L_1(x) = x; \\ (n+1)L_{n+1}(x) = (2n+1)xL_n(x) - nL_{n-1}(x) \end{cases} \quad (22)$$

187 They are orthogonal on standard interval $[-1, 1]$ with a constant weight function $\rho(x) \equiv 1$. The zeros
 188 of the Legendre polynomial $\boldsymbol{\xi} = \{\xi_i\}$, which are already defined according to the polynomial
 189 expression, can be used as samples in the uncertain parameter space due to their distribution structure.

190 It is worth mentioning that approximation of the uncertain response via the Gauss-Legendre quadrature
 191 will not be adopted due to the complexity in deduction. Instead, a regression form involving less
 192 mathematic efforts will be outlined. Suppose there are m uncertain parameters, we can predefine a p -
 193 order regression model for the uncertain response in a way similar to the response surface method

$$194 \quad f(\boldsymbol{\alpha}) = \sum_{k=0}^p \boldsymbol{\varphi}^{(k)} \mathbf{S}^{(k)}(\boldsymbol{\alpha}) \quad (23)$$

195 where $\boldsymbol{\varphi}^{(k)}$ is the unknown coefficient vector with the same size of $\mathbf{S}^{(k)}$. $\mathbf{S}^{(k)}$ is the vector for all
 196 the combinations of terms $\alpha_1^{i_1} \alpha_2^{i_2} \cdots \alpha_m^{i_m}$ satisfying

$$197 \quad \sum_{j=1}^m i_j = i_1 + i_2 + \cdots + i_m = k \quad (24)$$

198 We have $\mathbf{S}^{(0)} = [1]$ and

$$199 \quad \begin{cases} \mathbf{S}^{(1)} = [\alpha_1, \alpha_2, \cdots, \alpha_{m-1}, \alpha_m]^T \\ \mathbf{S}^{(2)} = [\alpha_1^2, \alpha_1\alpha_2, \alpha_1\alpha_3, \cdots, \alpha_m^2]^T \\ \vdots \\ \mathbf{S}^{(p)} = [\alpha_1^p, \alpha_1^{p-1}\alpha_2, \alpha_1^{p-1}\alpha_3, \cdots, \alpha_m^p]^T \end{cases} \quad (25)$$

200 In Eq. (23), the coefficient vector $\boldsymbol{\varphi} = [\boldsymbol{\varphi}^{(1)}, \boldsymbol{\varphi}^{(2)}, \cdots, \boldsymbol{\varphi}^{(p)}]$ should be determined to fully construct
 201 the model. The dimension of vector $\boldsymbol{\varphi}$ is $\tilde{n} = (m+p)! / m! p!$. Let $\mathbf{S} = [1, \mathbf{S}^{(1)}, \mathbf{S}^{(2)}, \cdots, \mathbf{S}^{(p)}]^T$, it
 202 further leads to the following expression

$$203 \quad f(\boldsymbol{\alpha}) = \boldsymbol{\varphi} \mathbf{S}(\boldsymbol{\alpha}) \quad (26)$$

204 For each uncertainty indicator α_i , the least number of collocations should be $n' = p+1$. These
 205 collocations can be generated by the zeros of the n' -order Legendre polynomial. In problems with
 206 single uncertainty, all the collocations should be used to estimate the unknown coefficients. When
 207 multiple uncertainties are taken into consideration, strategies aimed to reduce the computational efforts
 208 should be introduced. It was proposed that $2\tilde{n}$ collocations, i.e. two times of the dimension of $\boldsymbol{\varphi}$,
 209 will give robust results and achieve good efficiency (Isukapalli 1999; Wu et al. 2015). The collocations
 210 will be drawn randomly from the tensorial candidate space

$$211 \quad \hat{\boldsymbol{\xi}}_{2n \times m} \subset \{ \boldsymbol{\xi}_{1, n' \times 1} \otimes \boldsymbol{\xi}_{2, n' \times 1} \otimes \cdots \otimes \boldsymbol{\xi}_{m, n' \times 1} \} \quad (27)$$

212 At each collocation set $\hat{\xi}(j, 1:m)$, the deterministic harmonic solution can be evaluated by Eq. (15)
 213 as

$$214 \quad \hat{\mathbf{X}} = \{\hat{\mathbf{X}}_j, j = 1, 2, \dots, 2\tilde{n}\} \quad (28)$$

$$215 \quad \hat{\mathbf{X}}_j(\hat{\xi}_j) = \mathbf{H}^{-1}(\hat{\xi}_j)\Gamma(\hat{\xi}_j) \quad (29)$$

216 It should be noted that Eq. (29) represents a deterministic simulation as the uncertain parameters are
 217 all specified to fixed collocations. As a non-intrusive scheme, this is the only step where the rotor system
 218 model is involved and the deterministic modelling of the misalignment faults in Section 2 is integrated
 219 into the uncertainty propagation procedure. In other words, they are actually working independently
 220 and no further modifications to the established solver are needed in different uncertain cases. At the
 221 same time, the sample outputs of the \mathbf{S} matrix should be calculated

$$222 \quad \hat{\mathbf{S}} = \{\hat{\mathbf{S}}_j, j = 1, 2, \dots, 2\tilde{n}\} \quad (30)$$

$$223 \quad \hat{\mathbf{S}}_j(\hat{\xi}_j) = [1, \mathbf{S}^{(1)}(\hat{\xi}_j), \mathbf{S}^{(2)}(\hat{\xi}_j), \dots, \mathbf{S}^{(p)}(\hat{\xi}_j)]^T \quad (31)$$

224 Then, the unknown coefficient vector $\boldsymbol{\varphi}$ can be estimated in regression form as

$$225 \quad \boldsymbol{\varphi} = \hat{\mathbf{X}}\hat{\mathbf{S}}(\hat{\mathbf{S}}^T\hat{\mathbf{S}})^{-1} \quad (32)$$

226 The simplex meta-function of Eq. (26) is completely determined as long as the unknown coefficient
 227 vector is obtained. Ranges of the uncertain harmonic solutions can be easily estimated by this simple
 228 and explicit mathematical expression with respect to the standard variable vector $\boldsymbol{\alpha}$. The calculation
 229 performance will be assessed in the numerical simulation section and verifications will be provided.

230 **4. Numerical results with case studies**

231 In this section, numerical simulations regarding different uncertain parameters are carried out to
 232 investigate their effects on the vibration behaviours of the misaligned rotor. Here, only the model of the
 233 second rotor is presented as the first is rigid. Figure 3 shows the academic model of the rotor, which
 234 consists two rigid discs and is supported by two bearings at the two ends. It is discretized into 14 Euler
 235 beam elements with the torsional vibration being neglected. The two discs are located at node 3 and 12.
 236 The values of the model parameters are given in Table 1. Mass imbalance is considered at disc 2 and
 237 the rest of the rotor system is assumed to be well-balanced. All the responses will be drawn at node 2.
 238 The deterministic parallel misalignment is 0.001 m and the angular misalignment is 0.001 rad.

239 Firstly, the uncertainty in parallel misalignment is investigated. The varying range is taken as 10% of
 240 its mid-value. The uncertain results of the first four harmonic components using the 3-order surrogate
 241 procedure are demonstrated in Fig. 4. As clearly indicated in Fig. 4, the uncertainty in the parallel
 242 misalignment affects mainly the first order harmonic component and a small variability is noticed in
 243 the $3\times$ component. In the $2\times$ and $4\times$ components, the upper and lower response bounds stay
 244 close to the deterministic lines and no obvious response ranges are noticed. The results can be explained
 245 by referring to Eq. (7), which shows that the parallel misalignment will add a first-order harmonic force
 246 to the rotor system. The trivial variability in the third component is introduced by the coupling of the

247 first order and the third order components, which can be observed when applying the HBM.
248 It is important to validate the accuracy of the obtained uncertainty propagation results. To this end, the
249 scanning method is used to provide reference solutions using 100 equally spaced samples in the interval
250 of uncertain parallel misalignment. To validate the accuracy, it will be difficult to identify the differences
251 in the response bound curves between the reference solutions and those from the surrogate method since
252 they are very close to each other. Instead, the difference rate diagram for the upper and lower bounds is
253 provided by taking the reference solutions as accurate ones, as shown in Fig. 5. The magnitudes of
254 difference rates in Fig. 5 for the UB and LB demonstrate that the two categories of results are almost
255 identical for the $2\times$ and $4\times$ components. The largest rates appear in the $1\times$ and $3\times$ components,
256 but they are actually small (less than 1%). The simulation tasks are carried out on a personal laptop
257 operating Windows 10 with Intel Core i7-8550U@1.8GHz and 16GB RAM. The average CPU time for
258 the proposed Legendre method is 69.55 s whilst for the scanning method it is 3766.72 s. The calculation
259 efficiency is verified by this comparison. In fact, the deterministic model will be evaluated for every
260 sample to gather all the sample harmonic responses. The advantage will be significant if the rotor model
261 has many degrees of freedom. Thus, the effectiveness of the proposed method is validated.

262 Figure 6 presents the influence of 5% bounded uncertainty in the angular misalignment on the harmonic
263 responses of the rotor system. An obvious phenomenon contrary to that in the case of uncertain parallel
264 misalignment can be seen. In Fig. 6, variabilities of the responses only appear at the $2\times$ and $4\times$
265 components whilst no visible fluctuations are observed in the $1\times$ and $3\times$ components, which can be
266 evidenced by Eqs. (10) and (11). The effects of angular misalignment are expressed in second order
267 harmonic form and coupling effects will be introduced. Furthermore, the case with multi uncertainties
268 in different physical parameters is considered. Using the same 3-order surrogate, Fig. 7 gives the
269 variability of the vibration response of the rotor system under 5% uncertainties in both the
270 misalignments, 10% uncertainty in the unbalance and 2% uncertainty in the stiffness of bearing 2. With
271 those multiple uncertainties present, the traditional sampling-based scanning method will be
272 computationally prohibitive due to the geometrical growing samples. However, the bounds of the
273 harmonic components in Fig. 7 are smooth which shows the robustness of the surrogate. The variability
274 of dynamic response also indicates that the propagation of uncertainties causes significant deviations in
275 the deterministic harmonic solutions. As expected, all of the four harmonic components are affected by
276 the multiple uncertain parameters.

277 **5. Conclusions**

278 A finite element rotor model with both parallel and angular misalignments is considered in this paper
279 to investigate the propagation of non-probabilistic uncertainties in the dynamic responses. The HBM
280 coupled with a non-intrusive Legendre collocation based surrogate method is used to obtain the ranges
281 of the harmonic solutions. The uncertainty in parallel misalignment propagates only into the $1\times$ and

282 $3\times$ components whilst the uncertainty in angular misalignment affects the $2\times$ and $4\times$ components.
283 Multi uncertainties will demonstrate significant influences on all of the harmonic components of the
284 dynamic responses. Moreover, the effectiveness of the proposed method is validated via the scanning
285 method. The method is also suitable for the uncertainty analysis of general engineering structures.

286 **Acknowledgements**

287 This work is financially supported by the National Natural Science Foundation of China (No. 11272257)
288 and the Fundamental Research Funds for the Central Universities (No. 3102018ZY016).

289 **References**

- 290 Al-Hussain, K.M.: Dynamic stability of two rigid rotors connected by a flexible coupling with angular
291 misalignment. *J. Sound Vib.* **266**(2), 217-234 (2003)
- 292 Biswas, D., Ray, M.C.: Active constrained layer damping of geometrically nonlinear vibration of rotating
293 composite beams using 1-3 piezoelectric composite. *Int. J. Mech. Mater. Des.* **9**(1), 83-104 (2013)
- 294 Bhattacharya, A., Dutt, J.K., Pandey, R.K.: Influence of hydrodynamic journal bearings with multiple slip zones
295 on rotordynamic behavior. *J. Tribol.* **139**(6), 061701 (2017)
- 296 Didier, J., Sinou, J.-J., Faverjon, B.: Study of the non-linear dynamic response of a rotor system with faults and
297 uncertainties. *J. Sound Vib.* **331**(3), 671-703 (2012a)
- 298 Didier, J., Faverjon, B., Sinou, J.-J.: Analysing the dynamic response of a rotor system under uncertain parameters
299 by polynomial chaos expansion. *J. Vib. Control* **18**(5), 712-732 (2012b)
- 300 El-Mongy, H.H., Younes, Y.K.: Vibration analysis of a multi-fault transient rotor passing through sub-critical
301 resonances. *J. Vib. Control* **24**(14), 2986-3009 (2018)
- 302 Elishakoff, I., Sarlin, N.: Uncertainty quantification based on pillars of experiment, theory, and computation. Part
303 II: Theory and computation. *Mech. Syst. Signal Process* **74**, 54-72 (2016)
- 304 Friswell, M.I., Penny, J.E., Lees, A.W., Garvey, S.D.: Dynamics of rotating machines. Cambridge University Press,
305 2010.
- 306 Fu, C., Ren, X., Yang, Y., Xia, Y., Deng, W.: An interval precise integration method for transient unbalance
307 response analysis of rotor system with uncertainty. *Mech. Syst. Signal Process* **107**, 137-148 (2018a)
- 308 Fu, C., Ren, X., Yang, Y., Lu, K., Wang, Y.: Nonlinear response analysis of a rotor system with a transverse
309 breathing crack under interval uncertainties. *Int. J. Nonlin. Mech.* **105**, 77-87 (2018b)
- 310 Fu, C., Ren, X., Yang, Y., Qin, W.: Dynamic response analysis of an overhung rotor with interval uncertainties.
311 *Nonlinear Dynam.* **89**(3), 2115-2124 (2017)
- 312 Isukapalli, S.S.: Uncertainty analysis of transport-transformation models. The State University of New Jersey,
313 New Brunswick (1999)
- 314 Jiang, C., Lu, G., Han, X., Liu, L.: A new reliability analysis method for uncertain structures with random and
315 interval variables. *Int. J. Mech. Mater. Des.* **8**(2), 169-182 (2012)
- 316 Koroishi, E.H., Cavalini Jr, A.A., Lima, A.M., Steffen Jr, V.: Stochastic modeling of flexible rotors, *J. Braz. Soc.*
317 *Mech. Sci.* **34**, 574-583 (2012)
- 318 Kang, C.H., Hsu, W.C., Lee, E.K., Shiau, T.N.: Dynamic analysis of gear-rotor system with viscoelastic supports
319 under residual shaft bow effect. *Mech. Mach. Theory* **46**(3), 264-275 (2011)
- 320 Lu, K., Jin, Y., Chen, Y., Yang, Y., Hou, L., Zhang, Z., Li, Z., Fu, C.: Review for order reduction based on proper
321 orthogonal decomposition and outlooks of applications in mechanical systems. *Mech. Syst. Signal Process*
322 **123**, 264-297 (2019)

323 Lu, K., Lian, Z., Gu, F., Liu, H.: Model-based chatter stability prediction and detection for the turning of a flexible
324 workpiece. *Mech. Syst. Signal Process* **100**, 814-826 (2018)

325 Li, B., Ma, H., Yu, X., Zeng, J., Guo, X., Wen, B.: Nonlinear vibration and dynamic stability analysis of rotor-
326 blade system with nonlinear supports. *Arch. Appl. Mech.* **89**(7), 1375-1402 (2019)

327 Li, Z., Jiang, J., Tian, Z.: Stochastic dynamics of a nonlinear misaligned rotor system subject to random fluid-
328 induced forces. *J. Comput. Nonlin. Dyn.* **12**(1), 011004 (2017)

329 Li, Z., Jiang, J., Tian, Z.: Non-linear vibration of an angular-misaligned rotor system with uncertain parameters.
330 *J. Vib. Control* **22**(1), 129-144 (2016)

331 Li, J., Hong, J., Ma, Y., Zhang, D.: Modelling of misaligned rotor systems in aero-engines, in: ASME Turbo Expo
332 2012: International Mechanical Engineering Congress and Exposition, American Society of Mechanical
333 Engineers, 535-543 (2012)

334 Liu, J., Sun, X., Meng, X., Li, K., Zeng, G., Wang, X.: A novel shape function approach of dynamic load
335 identification for the structures with interval uncertainty. *Int. J. Mech. Mater. Des.* **12**(3), 375-386 (2016)

336 Lees, A.: Misalignment in rigidly coupled rotors. *J. Sound Vib.* **305**(1), 261-271 (2007)

337 Ma, H., Zeng, J., Feng, R., Pang, X., Wang, Q., Wen, B.: Review on dynamics of cracked gear systems. *Eng. Fail.*
338 *Anal.* **55**, 224-245 (2015a)

339 Ma, H., Wang, X., Niu, H., Wen, B.: Oil-film instability simulation in an overhung rotor system with flexible
340 coupling misalignment. *Arch. Appl. Mech.* **85**(7), 893-907 (2015b)

341 Nayfeh, A.H., Mook, D.T.: *Nonlinear oscillations*. John Wiley & Sons, 2008.

342 Patel, T.H., Darpe, A.K.: Vibration response of misaligned rotors. *J. Sound Vib.* **325**(3), 609-628 (2009)

343 Qi, W., Qiu, Z.: A collocation interval analysis method for interval structural parameters and stochastic excitation.
344 *Sci. China Phys. Mech.* **55**(1), 66-77 (2012)

345 Qiu, Z., Wang, X.: Comparison of dynamic response of structures with uncertain-but-bounded parameters using
346 non-probabilistic interval analysis method and probabilistic approach. *Int. J. Solids Struct.* **40**(20), 5423-
347 5439 (2003)

348 Redmond, I.: Study of a misaligned flexibly coupled shaft system having nonlinear bearings and cyclic coupling
349 stiffness-Theoretical model and analysis. *J. Sound Vib.* **329**(6), 700-720 (2010)

350 Roy, P.A., Meguid, S.A.: Nonlinear transient dynamic response of a blade subject to a pulsating load in a decaying
351 centrifugal force field. *Int. J. Mech. Mater. Des.* **14**(4), 709-728 (2018)

352 Ritto, T.G., Lopez, R.H., Sampaio, R., Cursi, J.E.S.D.: Robust optimization of a flexible rotor-bearing system
353 using the Campbell diagram. *Eng. Optimiz.* **43**(1), 77-96 (2011)

354 Soize, C.: Maximum entropy approach for modeling random uncertainties in transient elastodynamics. *J. Acoust.*
355 *Soc. Am.* **109**(5), 1979-1996 (2001)

356 Sinou, J.-J., Nechak, L., Besset, S.: Kriging metamodeling in rotordynamics: Application for predicting critical
357 speeds and vibrations of a flexible rotor. *Complexity*. Article ID 1264619 (2018)

358 Sinou, J.-J., Faverjon, B.: The vibration signature of chordal cracks in a rotor system including uncertainties. *J.*
359 *Sound Vib.* **331**(1), 138-154 (2012)

360 Sinha, J.K., Lees, A., Friswell, M.I.: Estimating unbalance and misalignment of a flexible rotating machine from
361 a single run-down. *J. Sound Vib.* **272**(3-5), 967-989 (2004)

362 Srinivas, R.Siva, Tiwari, R., Kannababu, Ch.: Model based analysis and identification of multiple fault parameters
363 in coupled rotor systems with offset discs in the presence of angular misalignment and integrated with an
364 active magnetic bearing. *J. Sound Vib.* **450**, 109-140 (2019)

365 Tai, X., Ma, H., Liu, F., Liu, Y., Wen, B.: Stability and steady-state response analysis of a single rub-impact rotor
366 system. *Arch. Appl. Mech.* **85**(1), 133-148 (2015)

367 Tuckmantel, F.W., Cavalca, K.L.: Vibration signatures of a rotor-coupling-bearing system under angular
368 misalignment. *Mech. Mach. Theory* **133**, 559-583 (2019)

369 Wang, N., Jiang, D.: Vibration response characteristics of a dual-rotor with unbalance-misalignment coupling
370 faults: Theoretical analysis and experimental study. *Mech. Mach. Theory* **125**, 207-219 (2018)

371 Wang, C., Ma, Y., Zhang, D., Hong, J.: Interval analysis on aero-engine rotor system with misalignment, in: ASME
372 Turbo Expo 2015: Turbine Technical Conference and Exposition, American Society of Mechanical Engineers,
373 V07AT30A002 (2015)

374 Wu, J., Luo, Z., Zheng, J., Jiang, C.: Incremental modeling of a new high-order polynomial surrogate model. *Appl.*
375 *Math. Model.* **40**(7-8), 4681-4699 (2016)

376 Wu, J., Luo, Z., Zhang, N., Zhang, Y.: A new interval uncertain optimization method for structures using
377 Chebyshev surrogate models. *Comput. Struct.* **146**, 185-196 (2015)

378 Wu, J., Zhang, Y., Chen, L., Luo, Z.: A Chebyshev interval method for nonlinear dynamic systems under
379 uncertainty. *Appl. Math. Model.* **37**(6), 4578-4591 (2013)

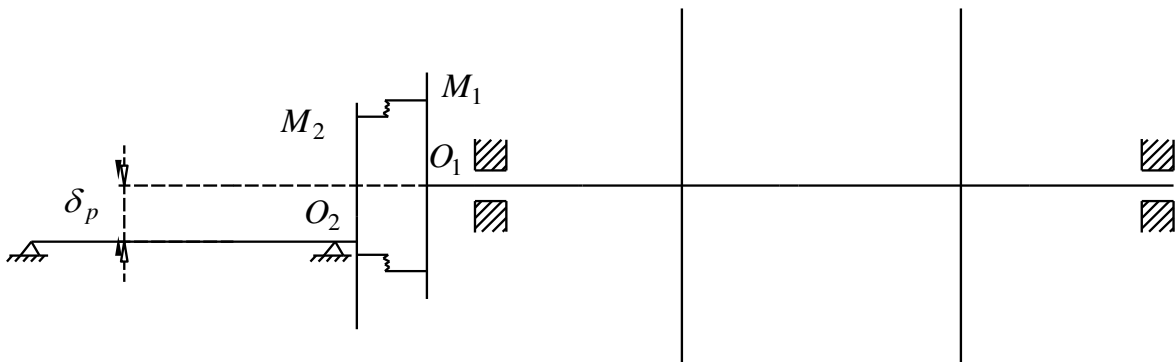
380 Xu, M., Marangoni, R.: Vibration analysis of a motor-flexible coupling-rotor system subject to misalignment and
381 unbalance, Part II: experimental validation. *J. Sound Vib.* **176**(5), 681-691 (1994)

382 Yang, Y., Wu, Q., Wang, Y., Qin, W., Lu, K.: Dynamic characteristics of cracked uncertain hollow-shaft. *Mech.*
383 *Syst. Signal Process* **124**, 36-48 (2019)

384

385 **List of Figures**

386

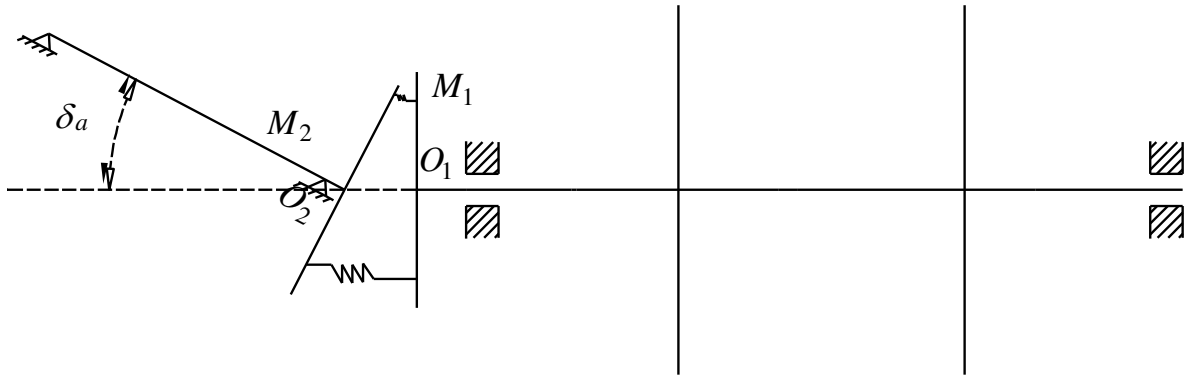


387

388

389

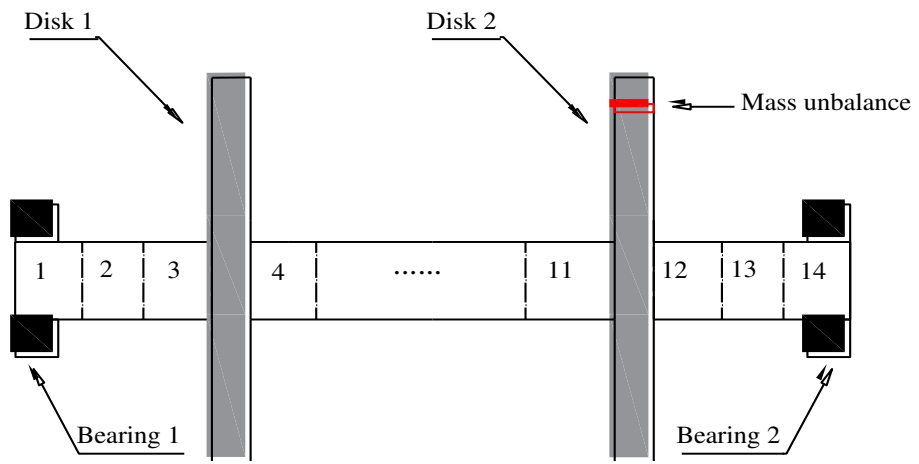
Figure 1. Schematic diagram of parallel misalignment.



390
 391
 392

Figure 2. Schematic diagram of angular misalignment.

393



394

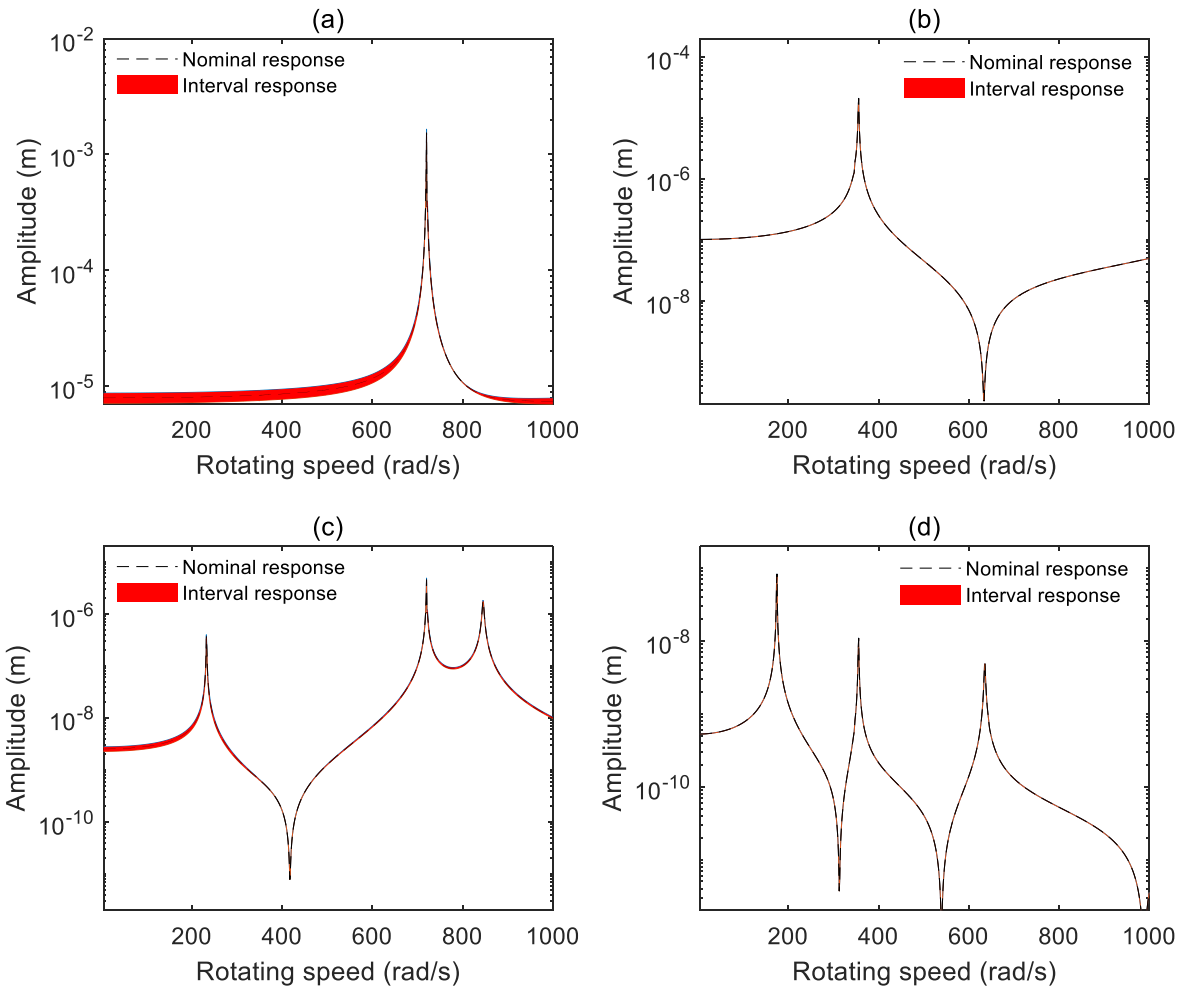
395

396

397

Figure 3. Academic model of the rotor system.

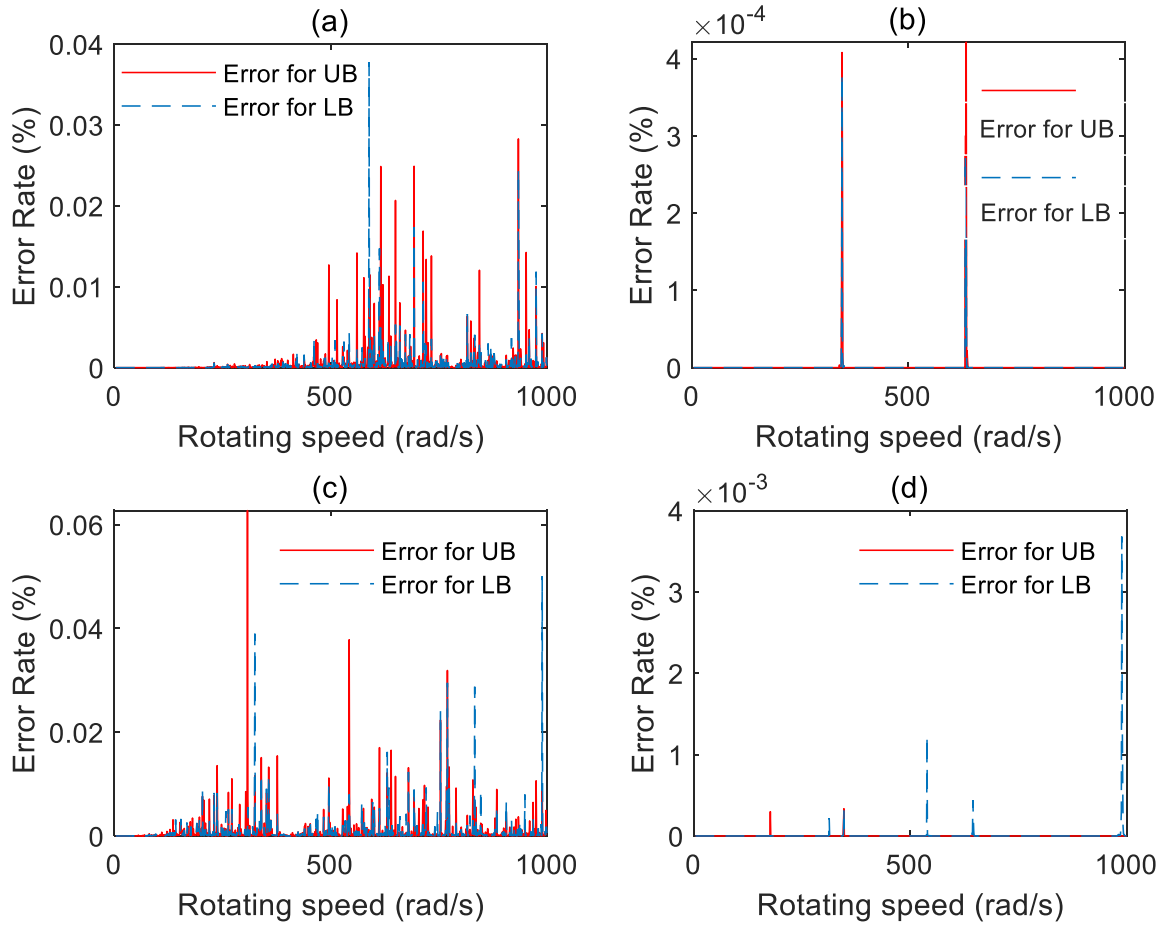
398



399

400 **Figure 4.** Response variability under 10% uncertainty in parallel misalignment: (a) $1\times$ harmonic
 401 component, (b) $2\times$ harmonic component, (c) $3\times$ harmonic component, (d) $4\times$ harmonic
 402 component.

403



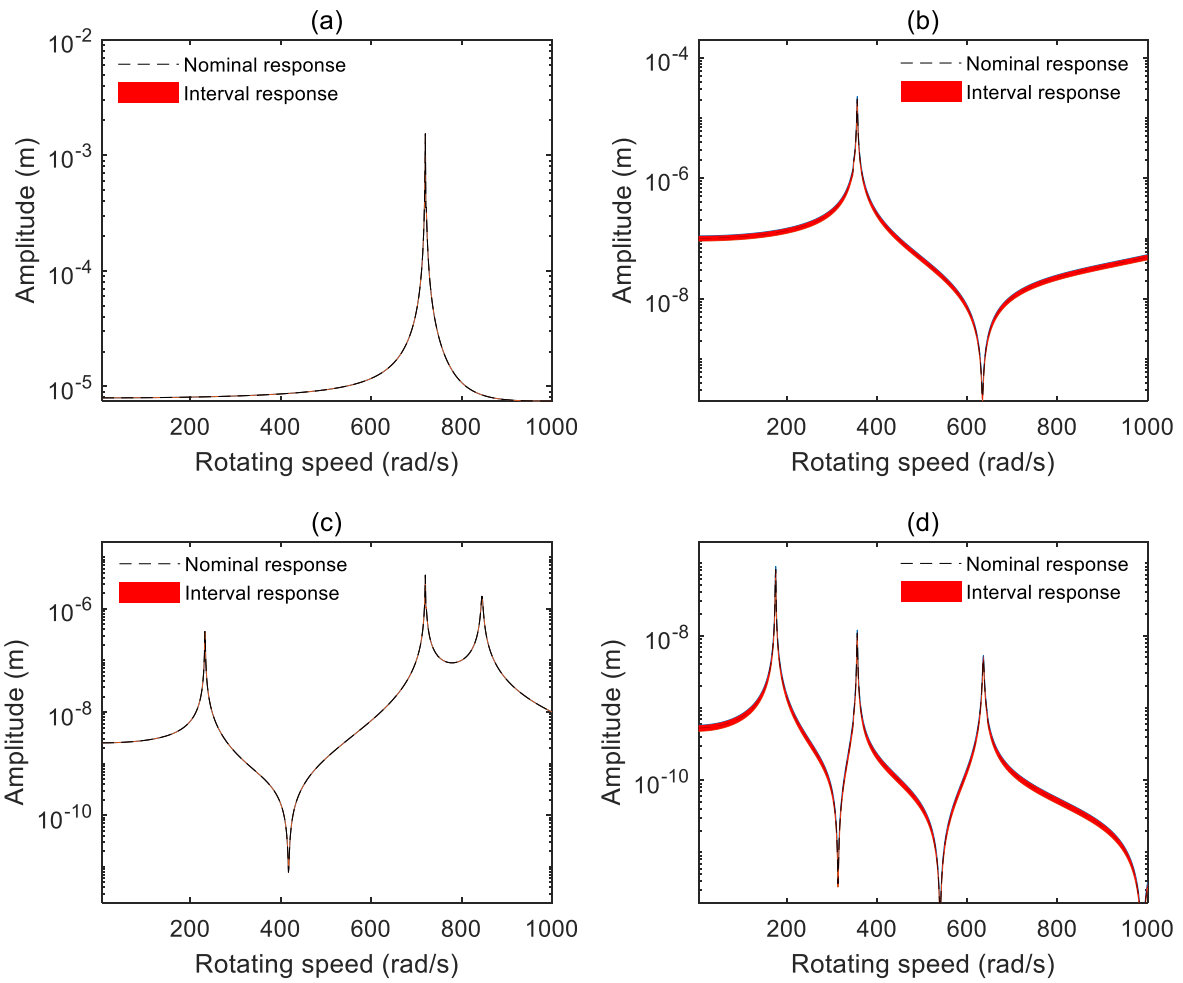
404

405

406

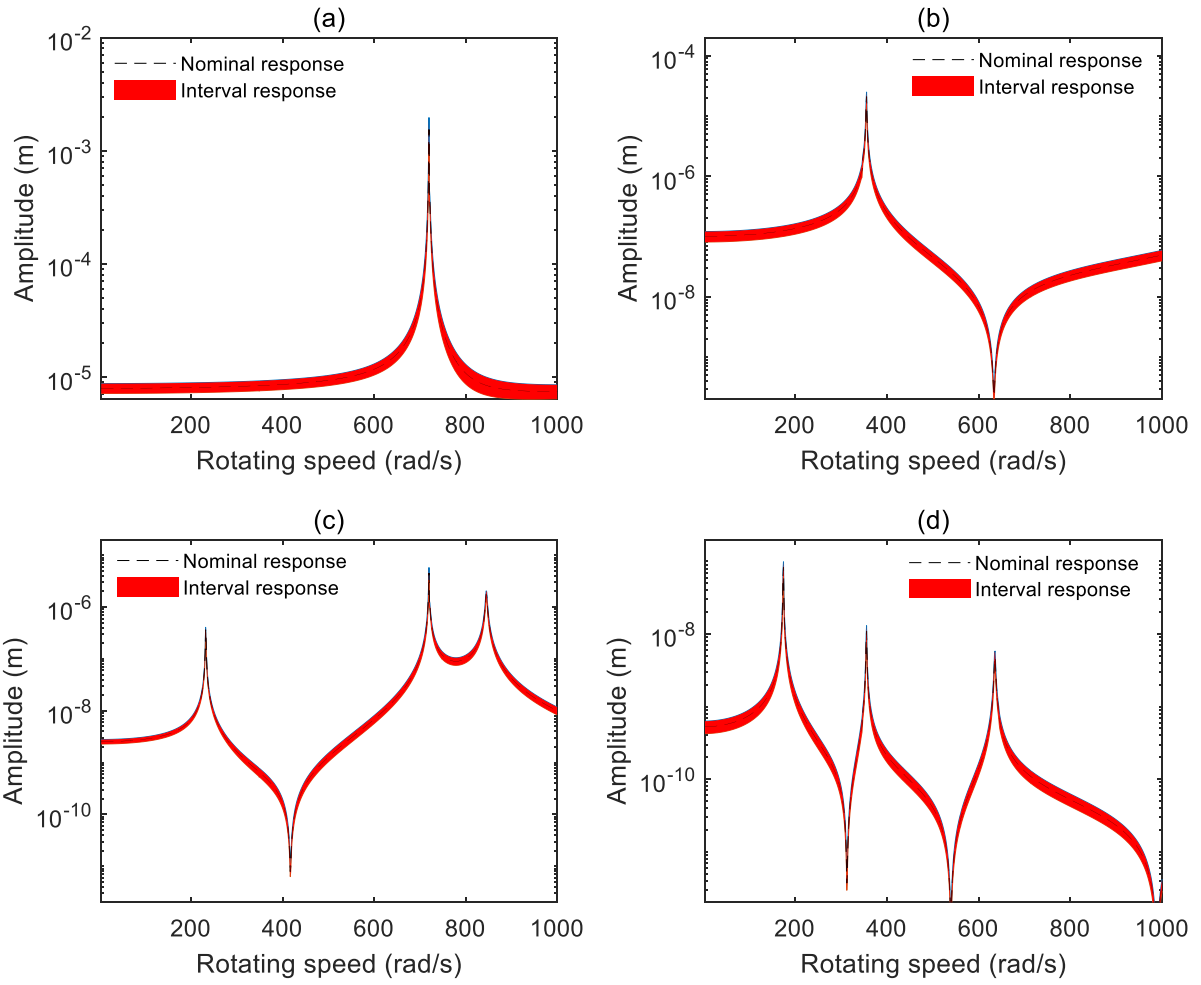
407

Figure 5. Calculation error rate: (a) $1\times$ harmonic component, (b) $2\times$ harmonic component, (c) $3\times$ harmonic component, (d) $4\times$ harmonic component.



408
 409
 410
 411
 412

Figure 6. Response variability under 5% uncertainty in angular misalignment: (a) $1\times$ harmonic component, (b) $2\times$ harmonic component, (c) $3\times$ harmonic component, (d) $4\times$ harmonic component.



413

414

415

416

Figure 7. Response variability under multiple uncertainties: (a) $1\times$ harmonic component, (b) $2\times$ harmonic component, (c) $3\times$ harmonic component, (d) $4\times$ harmonic component.

417 **List of Tables**

418

419 **Table 1.** Values of parameters

Parameter	Value	Parameter	Value
Length of shaft, l	0.825 m	Young's modulus, E	2.1×10^{11} N/m ²
Axial stiffness of bolts, k_a	2×10^5 N/m	Density, ρ	7800 kg/m ³
Transverse stiffness of bolts, k_t	1×10^6 N/m	Viscous damping, C	200 N · s/m
Unbalance angle, φ	0 rad	Stiffness of bearing 1, K_1	7×10^7 N/m
Poisson's ratio, ν	0.3	Stiffness of bearing 2, K_2	7×10^7 N/m
Disk mass, m_d	0.5 kg	Mass unbalance, $m_e d$	5×10^{-5} kg · m
Radius of the disks, R_0	0.22 m	Additional stiffness, k'	1×10^6 N/m

420

421